Direct SAR Mapping by Thermoacoustic Imaging: Experimental Proof-of-Concept

Simone Angela Winkler[1], Paul Picot[2], Michael Thornton[2], and Brian K Rutt[1]
[1]*Dept. of Radiology, Stanford University, Stanford, CA, United States,* [2]*Endra Inc., Ann Arbor, Michigan, United States*

Target Audience: MR scientists and engineers with focus on high field safety monitoring and assessment.

Purpose: We propose a new concept for direct measurement of specific absorption rate (SAR), to be used as a safety assessment/monitoring tool for MRI. The concept involves the use of short bursts of RF energy and the measurement of the resulting thermoacoustic excitation pattern by an array of ultrasound transducers, followed by image reconstruction to yield the 3D SAR distribution. Proof of concept has previously been shown by simulation [1]; here we present first experimental proof-of-principle of direct SAR mapping by thermoacoustic imaging.

Methods: SAR is a key safety consideration in high field MRI, given the potential for tissue damage at locations of SAR hotspots. To date, no practical methods to measure local SAR *in vivo* exist; the only quantity that is routinely measured is average (global) SAR. Thermoacoustic signals are ultrasound waves generated through the absorption of pulsed or modulated RF/microwave energy. A high intensity RF source is used to irradiate the tissue using short RF pulses, and absorbed RF energy then causes thermoelastic expansion with resulting pressure waves. In particular, for short pulses, the pressure wave equation is directly related to the SAR as follows: $\left[\nabla^2 - \frac{1}{v_s^2}\frac{\partial^2}{\partial t^2}\right] p = -\frac{\beta}{C_p}\widetilde{SAR}(\mathbf{r})\frac{\partial I}{\partial t}$ (1), where $p(\mathbf{r},t)$ is the acoustic pressure field, β is the volume expansion coefficient, v_s is the speed of sound, and C_p is the thermal capacity of the tissue. The quantities $\widetilde{SAR}(\mathbf{r}) = \frac{\sigma(\mathbf{r})E(\mathbf{r})^2}{\rho(\mathbf{r})}$ (2) and $I(t)$ are the spatially varying SAR pattern and the unitless RF pulse temporal modulation, respectively. Guided by the above theory, we propose to use thermoacoustic imaging to map SAR, using the MRI system's RF transmit coil for delivery of the pulsed RF energy, and an ultrasonic transducer array to detect the thermoacoustic signals. The above governing equation can then be solved for $\widetilde{SAR}(\mathbf{r})$ assuming measurement of $p(t)$ at a number of locations surrounding the body, and assuming knowledge of all other equation parameters.

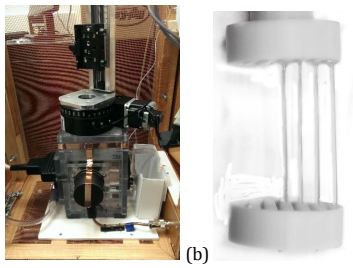

(a) (b)

Fig. 1 (a) Experimental thermoacoustic system available for proof of concept, (b) phantom construction: saline concentrations in phantom I: 2.25% in all tubes; in phantom II: from center to outer edge: 5%, 3%, 2.25%, 1.25%.

Experimental proof of concept: An in-vitro experimental proof of concept was carried out using a prototype thermoacoustic imaging system (Fig. 1a). This system operates at an RF frequency of 434 MHz and is therefore suitable for mimicking the field variations that we would observe in a human UHF MR scanner, as 434 MHz corresponds to a field strength of approximately 10T. The system consists of two RF channels with a peak power of 5 kW each, exciting a standing wave electromagnetic field pattern by means of two horn antennas located on opposite sides of the tank. A pulse train with 70 ns pulse rise time, 180 ns pulse width, and pulse repetition rate of 2 kHz was used. Thermoacoustic signals were then acquired using a 128-element ultrasound transducer array (using a 3-dB bandwidth of 2 MHz, centered at 3 MHz), situated at the front of the tank. Reconstruction was performed using an advanced backprojection algorithm.

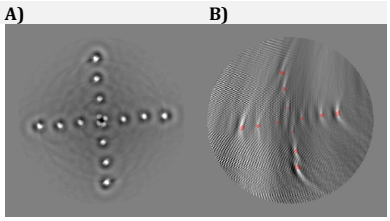

Fig. 2 Thermoacoustic images for (a) constant and (b) spatially varying conductivity and *E*-field.

In order to prove experimental feasibility of in-vivo SAR mapping, two experiments were carried out using spatially constant (experiment A) and spatially varying (experiment B) SAR distributions. These two conditions were achieved using spatially constant conductivity and *E*-field (experiment A)_and spatially varying conductivity and *E*-field (experiment B). To this end we constructed two phantoms from a single-row grid of saline tubes, equally spaced at a distance of 5 mm in a 3D-printed holder (see Fig. 1b): phantom I had inclusions of constant conductivity (using four saline tubes of equal 5% saline concentration), and phantom II had inclusions of varying conductivity (saline concentrations of 5%, 3%, 2.25%, 1.25%, from edge to center). Constant vs spatially varying *E*-fields were achieved by exciting both or only one of the two horn antennas, respectively. Additionally, to improve the constant *E*-field pattern for experiment A, the phantom was rotated around the center of the field of view (FOV) to spatially average its *E*-field exposure. Phantom images were acquired with the row of tubes pointing in each of the four principal directions to cover a wide range of field variations; resulting images were summed and yielded a crosshair pattern of tubes. (Fig. 2A) The average image value for each tube was then measured and compared to the theoretical SAR. The *E*-field amplitudes for the SAR calculation in (2) were measured using a coaxial field probe connected to an oscilloscope. All values were adjusted for constant background image noise and then normalized to the SAR value of the central tube.

TABLE I
SAR VALUES FOR EXPERIMENT A

pos. (mm)	Horizontal SAR (theory)	Horizontal SAR (exp)	% err	Vertical SAR (theory)	Vertical SAR (exp)	% err
-15	1.00	1.01	1	1.00	0.87	13
-10	1.00	0.99	1	1.00	0.85	15
-5	1.00	0.95	5	1.00	0.85	15
0	1.00	1.00	0	1.00	1.00	0
5	1.00	0.98	2	1.00	0.87	13
10	1.00	1.11	11	1.00	1.09	9
15	1.00	1.09	9	1.00	1.13	13

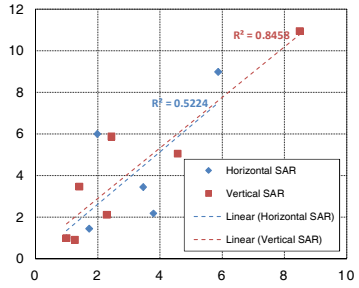

Fig. 3 Theoretical vs. experimental SAR values for experiment B.

Results: The thermoacoustic images resulting from the two in-vitro experiments are shown in Fig. 2. Table I shows the corresponding image values for experiment A in comparison to the theoretical relative SAR, with % errors shown. It is seen that in experiment A, SAR errors are low, confirming the uniformity of direct thermoacoustic SAR mapping over the field of view. Remaining errors are attributed to remaining variations in the *E*-field due to field amplitude variations within the standing wave pattern. Experiment B represents a more realistic scenario; results in Fig. 3 shows good correlation between theory and experiment (r^2 = 0.52 for horizontal and r^2 = 0.85 for vertical SAR values).

Discussion: This study presents the first experimental evidence of the feasibility of thermoacoustic SAR mapping. Projecting toward future integration into a typical 7T MRI system, an RF transmitter with a peak power of 8 kW is available on most 7T scanners, and would yield an ultrasound pressure of approx. 1 Pa in a non-attenuated thermoacoustic experiment, which is realistically measurable. In our proposed lower resolution SAR mapping scenario, we expect that the skull will not pose a significant problem, assuming the use of ultrasound frequencies in the range of 200 kHz. This relatively low frequency can be selected to overcome ultrasound waveform aberration and absorption by the human skull, yet should still permit spatial resolution in the range of 1.5 cm in the resulting SAR maps.

Conclusion: A novel thermoacoustic method for in-vivo mapping of local SAR patterns in MRI has been proposed and verified in-vitro.

References: [1]Winkler SA, et al, Proc Int Soc Magn Res 22:4898 (2014)

Acknowledgement: Research support from NSERC, NIH (P41 EB015891 and 1 S10 RR026351-01Al), GE Healthcare.